

A fast and accurate numerical approach for electromagnetic inversion

Eleonora Denich* Paolo Novati † Stefano Picotti ‡

Abstract

This paper deals with the solution of Maxwell's equations to model the electromagnetic fields in the case of a layered earth. The integrals involved in the solution are approximated by means of a novel approach based on the splitting of the reflection term. The inverse problem, consisting in the computation of the unknown underground conductivity distribution from a set of modeled magnetic field components, is also considered. Two optimization algorithms are applied, based on line- and global-search methods, and a new minimization approach is presented. Several EM surveys from the ground surface are simulated, considering the horizontal coplanar (HCP) and perpendicular (PRP) magnetic dipolar configurations. The numerical experiments, carried out for the study of river-levees integrity, allowed to estimate the errors associated to these kind of investigations, and confirm the reliability of the technique.

1 Introduction

The aim of electromagnetic (EM) sounding methods in geophysics is to obtain information about the subsoil conductivity distribution, by recorded measurements of the EM field components. One technique consists in placing magnetic dipoles above the surface, composed of a transmitter coil and different couples of adjacent receiver coils. The receiver couples (i.e. dual coils) are placed at different distances (offsets) from the transmitter coil. The most common dipole geometry consists of transmitter and receiver loops that can be horizontal coplanar (HCP configuration) and perpendicular (PRP configuration). Among the available instruments, the DUALEM (DUAL-geometry Electro-Magnetic; <http://www.duallem.com>) system is often used. The receiver couples are placed at 2, 4, 6 and 8 m from the transmitter coil, and typical source-receiver geometries are the horizontal coplanar (HCP configuration) and perpendicular (PRP

*Dipartimento di Matematica e Geoscienze, Università di Trieste, eleonora.denich@phd.units.it

†Dipartimento di Matematica e Geoscienze, Università di Trieste, novati@units.it

‡Department of Geophysics, Istituto Nazionale di Oceanografia e di Geofisica Sperimentale (OGS), Borgo Grotta Gigante 42c, 34010 Sgonico, Trieste, Italy, spicotti@inogs.it

configuration) coils. The electromagnetic induction effect, encoded in the first-order linear differential Maxwell equations, produces eddy alternating currents in the soil which on their turn, induce response EM fields, that can be used to determine the conductivity profile of the ground.

For simplicity, the local subsurface structures below the DUALEM instrument can be assumed composed by horizontal and homogeneous layers. Under this assumption, general integral solutions of Maxwell equations (i.e., the EM fields) for vertical and horizontal magnetic dipoles, can be derived (see [29]) and represented as Hankel transforms of order l , as follows:

$$F(r, p) = \int_0^{\infty} f(\lambda, p) J_l(\lambda r) d\lambda, \quad (1)$$

where r is the offset and J_l is the Bessel function of the first kind of order l . The function $f(\lambda, p)$ contains the vector p characterizing the subsurface model parameters, i.e. the conductivity and the thickness of each layer. As for the Bessel functions we refer here to [30] for an overview. In the case of conductivities of geological materials, only the imaginary part of the complex function $F(r, p)$ is considered. Indeed, while the instruments (e.g., the DUALEM) used for experimental surveys collect both in-phase and quadrature measurements of the magnetic field components, the former become important only over highly conductive materials, and are particularly effective for locating confined conductors, such as metal bodies, or boulders of graphite or sulfide.

By a mathematical point of view, in general, the function $F(r, p)$ is not analytically computable and therefore it is necessary to employ a numerical scheme. Anyway, the slowly decay of the oscillations determined by the Bessel function makes the problem very difficult to handle, because traditional quadrature rules typically fail to converge. In order to numerically evaluate these kind of integrals, in 1971 Ghosh [10] introduced the digital filtering algorithm for the direct interpretation of geoelectrical resistivity soundings measurements. This method is essentially a standard quadrature rule, but the main difference is that the weights are computed by solving a linear equation obtained by imposing the rule to be correct on a set of training functions (not polynomials) for which the corresponding integral (1) is known (e.g., [15]).

In general, considering the change of variables $r = e^x$ and $\lambda = e^{-y}$, equation (1) becomes

$$e^x F(e^x, p) = \int_{-\infty}^{+\infty} f(e^{-y}, p) J_l(e^{x-y}) dy,$$

and can be rewritten as the convolution

$$\tilde{F}(x, p) = \int_{-\infty}^{+\infty} \tilde{f}(y, p) \tilde{J}_l(x - y) dy = \int_{-\infty}^{+\infty} \tilde{f}(x - y, p) \tilde{J}_l(y) dy,$$

where $\tilde{F}(x, p) = e^x F(e^x, p)$, $\tilde{f}(y, p) = f(e^{-y}, p)$ and $\tilde{J}_l(x - y) = J_l(e^{x-y})$. Then, given a set of training functions $\{f_k\}_{k=-N, \dots, N}$, the method consists in setting $2N + 1$ grid points $\lambda_j = e^{-jy}$, $j = -N, \dots, N$, and then prescribes to solve with

respect to the filter coefficients w_j , $j = -N, \dots, N$, the linear system

$$\tilde{F}_k(x, p) = \sum_{j=-N}^N \tilde{f}_k(x - y, p) w_j, \quad k = -N, \dots, N. \quad (2)$$

Finally, the resulting $2N + 1$ -points digital linear filter approximation of equation (1) is

$$F(r, p) \approx \frac{1}{r} \sum_{j=-N}^N f\left(\frac{\lambda_j}{r}, p\right) w_j. \quad (3)$$

Later, this algorithm has been reconsidered by many authors (see e.g. [3, 18, 21, 2, 15, 27, 14, 31]) to handle specific EM problems involving integrals of type (1), and improvements to the determination of filter coefficients have been developed (see [?, 22]). In particular, Koefoed and Dirks [?] proposed a Wiener-Hopf least-squares method, while Kong [22] uses the GMRES, to solve the linear system (2).

In this work we consider a different approach that is much simpler and reliable for integrals of type (1). Indeed, in this framework the function $f(\lambda, p)$ can be decomposed as $f_1(\lambda, p) + f_2(\lambda, p)$ in which $f_1(\lambda, p)$ is such that $F_1(r, p)$ is known exactly, and the oscillating function $f_2(\lambda, p)$ decays exponentially. For realistic sets of parameters, the oscillations are quite rapidly damped and the corresponding integral $F_2(r, p)$ can be accurately computed by a classical quadrature rule on finite intervals. We remark that the frequency of the oscillations increases with r , so that the integration of $F(r, p)$ becomes more difficult. In this view the splitting allows to reduce the sensitivity with respect to r . The idea of splitting the integral in two parts has originally been introduced in [17] where, however, the second integral is still approximated as in (3) by digital filtering, without exploiting the fast decay of the oscillations.

In order to reconstruct realistic subsurface structures from EM measurements, a tomographic approach is needed. A typical inversion approach consists in an iterative procedure involving the computation of the EM response of a layered model (forward modelling) and the solution of the inverse problem. The algorithm attempts to minimize the mismatch between the measured data and the predicted data, by updating the model parameters at each iteration. Having at disposal a reliable method for evaluating (1), here we also consider the inverse problem of computing the model parameters (i.e., conductivity and thickness of the layers) from a set of measured field values at different offsets. To this purpose we employ two optimization algorithms based on the BFGS line-search method ([4, 8, 12, 26]) and on the Simulated Annealing (SA) global-search technique ([19, 11]). In order to reduce as much as possible the number of integral evaluations, we also derive an analytic approximation of these integrals that can be used in the initial iterations of the tomographic procedure, to have a first estimate of the solution.

This paper is organized as follows. In Section 2 we define the integral formulations of the EM fields. Section 3 deals with the numerical approach used for the computation of the integrals. In Section 4 we derive useful approximations in the case of a layered earth. In Section 5 we introduce the inverse problem and

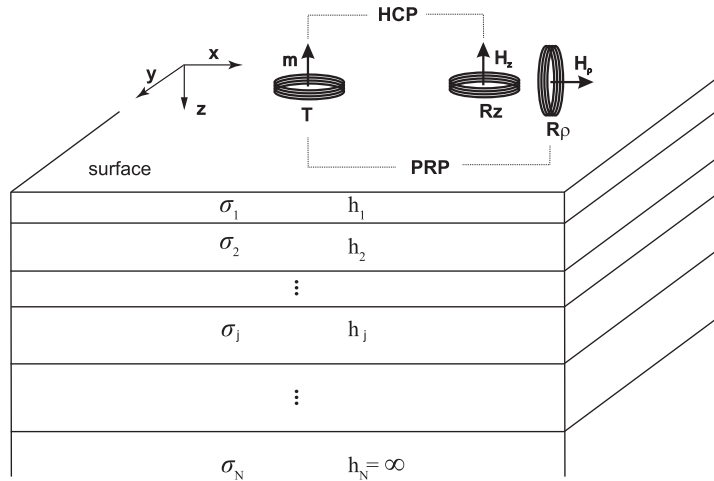


Figure 1: Layered underground conductivity model and dual-coil configuration inside the DUALEM instrument.

propose an optimization algorithm to reconstruct the underground conductivity distribution. Finally, in Section 6 we present some realistic examples of river levees conductivity models, and report the numerical results in the case of a 3-layered subsoil.

2 Definition of the forward model

Consider a layered underground model as in Figure 1, where σ_j and h_j , $j = 1, \dots, N$, represent conductivity and thickness of the j -th layer, respectively. The deeper layer is assumed to have infinite thickness. Let f and m be the transmitter's frequency and the magnetic moment, μ the magnetic permeability of vacuum and r the offset. The angular frequency is $\omega = 2\pi f$. In order to derive the mathematical formulation of the fields, it is convenient to introduce a cylindrical polar coordinate system (ρ, ϕ, z) , with the longitudinal axis downward directed, such that the ground plane coincides with the plane $z = 0$, the transmitter is located at the origin and the receiver is placed along the polar axis.

Let us consider the DUALEM instrument, for which the dipole geometry consists of a transmitter loop (T) and many dual receiver loops (Rz, Rρ) that are horizontal co-planar (HCP configuration) and perpendicular (PRP configuration). Figure 1 represents an example of dual-coil configuration inside the DUALEM, where the offset is 2 m and 2.1 m between T and the first couple of receivers Rz, Rρ, respectively. Other couples of receivers are located at 4, 6 and 8 m offset. In this setting, the theoretical components of the magnetic field at

the receiver location on the surface are given by (see [29] and [17])

$$H_z^{(N)} = \frac{m}{4\pi} \int_0^\infty (1 + R_0(\lambda)) \lambda^2 J_0(\lambda r) d\lambda, \quad (4)$$

$$H_\rho^{(N)} = \frac{m}{4\pi} \int_0^\infty (1 - R_0(\lambda)) \lambda^2 J_1(\lambda r) d\lambda, \quad (5)$$

for HCP and PRP configurations, respectively. In the above formulas $R_0(\lambda)$ is the reflection term, recursively defined by

$$\begin{aligned} R_0(\lambda) &= \frac{R_1(\lambda) + \Psi_1(\lambda)}{R_1(\lambda)\Psi_1(\lambda) + 1}, \\ R_j(\lambda) &= \frac{R_{j+1}(\lambda) + \Psi_{j+1}(\lambda)}{R_{j+1}(\lambda)\Psi_{j+1}(\lambda) + 1} e^{-2u_j(\lambda)h_j}, \quad j = 1, \dots, N-1, \\ R_N(\lambda) &= 0, \end{aligned} \quad (6)$$

where

$$\Psi_j(\lambda) = \frac{u_{j-1}(\lambda) - u_j(\lambda)}{u_{j-1}(\lambda) + u_j(\lambda)}, \quad j = 1, \dots, N,$$

in which $u_0(\lambda) = \lambda$ and $u_j(\lambda) = \sqrt{\lambda^2 - k_j^2}$, $k_j = \sqrt{-i\omega\mu\sigma_j}$, for $j = 1, \dots, N$. In order to avoid redundancies and to reduce the length of some formulas, in the sequel we simply write R_j , Ψ_j , u_j , in place of $R_j(\lambda)$, $\Psi_j(\lambda)$, $u_j(\lambda)$.

We observe that if $N = 1$, representing the situation of homogeneous earth, then $R_1 = 0$, $R_0 = \Psi_1$, and the integrals (4) e (5) can be exactly evaluated. Indeed, in [29] it is shown that in this situation

$$\begin{aligned} H_z^{(1)} &= \frac{m}{2\pi r} \frac{\partial}{\partial r} \left(r \int_0^\infty \frac{\lambda^2}{\lambda + u_1} J_1(\lambda r) d\lambda \right) \\ &= \frac{m}{2\pi r} \frac{\partial}{\partial r} \left(-r \frac{\partial}{\partial r} \int_0^\infty \frac{\lambda}{\lambda + u_1} J_0(\lambda r) d\lambda \right) \\ &= \frac{m}{2\pi r} \frac{\partial}{\partial r} \left(-r \frac{\partial}{\partial r} \int_0^\infty \frac{\lambda(\lambda - u_1)}{\lambda^2 - u_1^2} J_0(\lambda r) d\lambda \right) \\ &= \frac{m}{2\pi r k_1^2} \frac{\partial}{\partial r} \left(-r \frac{\partial}{\partial r} \left(\int_0^\infty \lambda^2 J_0(\lambda r) d\lambda - \int_0^\infty \lambda u_1 J_0(\lambda r) d\lambda \right) \right), \\ H_\rho^{(1)} &= \frac{m}{4\pi} \frac{\partial}{\partial r} \int_0^\infty \frac{\lambda - u_1}{\lambda + u_1} \lambda J_0(\lambda r) d\lambda \\ &= \frac{m}{4\pi} \frac{\partial}{\partial r} \int_0^\infty \frac{\lambda - u_1}{\lambda + u_1} \frac{\lambda + u_1}{\lambda + u_1} \lambda J_0(\lambda r) d\lambda \\ &= \frac{m k_1^2}{4\pi} \frac{\partial}{\partial r} \int_0^\infty \frac{\lambda}{(\lambda + u_1)^2} J_0(\lambda r) d\lambda. \end{aligned}$$

An analytical expression for the above integrals can be achieved by using [13,

p.707] and [7, Vol.2, pp.8-9] respectively, to obtain

$$H_z^{(1)} = \frac{m}{2\pi k_1^2 r^5} \left[9 - (9 + 9ik_1 r - 4k_1^2 r^2 - ik_1^3 r^3) e^{-ik_1 r} \right],$$

$$H_\rho^{(1)} = -\frac{mk_1^2}{4\pi r} \left[I_1 \left(\frac{ik_1 r}{2} \right) K_1 \left(\frac{ik_1 r}{2} \right) - I_2 \left(\frac{ik_1 r}{2} \right) K_2 \left(\frac{ik_1 r}{2} \right) \right],$$

where I_l e K_l are the modified Bessel functions of order l , of the first and second type respectively.

Defining, for $l = 0, 1$

$$g_l(\lambda) = (R_0 - \Psi_1) \lambda^2 J_l(\lambda r), \quad (7)$$

$$q_l(\lambda) = [1 + (-1)^l \Psi_1] \lambda^2 J_l(\lambda r), \quad (8)$$

we can write (see (4), (5))

$$(1 + R_0) \lambda^2 J_0(\lambda r) = g_0(\lambda) + q_0(\lambda),$$

$$(1 - R_0) \lambda^2 J_1(\lambda r) = q_1(\lambda) - g_1(\lambda).$$

Since $q_l(\lambda)$ represents the integrand function in the case $N = 1$ ($R_1 = 0$ and hence $g_l(\lambda) = 0$), we have that

$$\frac{m}{4\pi} \int_0^\infty q_0(\lambda) d\lambda = H_z^{(1)},$$

$$\frac{m}{4\pi} \int_0^\infty q_1(\lambda) d\lambda = H_\rho^{(1)},$$

and therefore

$$H_z^{(N)} = \frac{m}{4\pi} \int_0^\infty g_0(\lambda) d\lambda + H_z^{(1)}, \quad (9)$$

$$H_\rho^{(N)} = -\frac{m}{4\pi} \int_0^\infty g_1(\lambda) d\lambda + H_\rho^{(1)}. \quad (10)$$

3 Numerical computation of the fields

Our strategy for the computation of $H_z^{(N)}$ and $H_\rho^{(N)}$ in the general case of N layers is based on the observation that the functions $g_l(\lambda)$, $l = 0, 1$, exponentially decay with respect to λ . To prove this behavior, some preliminary results are necessary.

Lemma 1 *It holds*

$$R_0 - \Psi_1 = R_1 \left(1 + \mathcal{O} \left(\frac{1}{\lambda^2} \right) \right), \quad \text{as } \lambda \rightarrow +\infty.$$

Proof. Using the definitions of R_0 and Ψ_1 we have

$$R_0 - \Psi_1 = \frac{4R_1 u_1}{R_1 k_1^2 + (\lambda + u_1)^2} \lambda. \quad (11)$$

Since

$$u_1 = \lambda \sqrt{1 - \frac{k_1^2}{\lambda^2}} = \lambda \left(1 - \frac{k_1^2}{2\lambda^2} + \mathcal{O}\left(\frac{1}{\lambda^4}\right) \right),$$

as $\lambda \rightarrow +\infty$, we can write

$$\begin{aligned} R_0 - \Psi_1 &= \frac{4R_1 u_1 \lambda}{R_1 k_1^2 + (\lambda + u_1)^2} = \frac{4R_1 \lambda^2 \left(1 - \frac{k_1^2}{2\lambda^2} + \mathcal{O}\left(\frac{1}{\lambda^4}\right) \right)}{R_1 k_1^2 + \lambda^2 \left(2 - \frac{k_1^2}{2\lambda^2} + \mathcal{O}\left(\frac{1}{\lambda^4}\right) \right)^2} \\ &= R_1 \left(1 + \mathcal{O}\left(\frac{1}{\lambda^2}\right) \right). \end{aligned}$$

■

Lemma 2 *The function R_1 can be written in the following form*

$$R_1 = \sum_{k=1}^{N-1} \delta_k(\lambda) \exp(-\gamma_k \lambda), \quad (12)$$

where

$$\begin{aligned} \gamma_k &= \sum_{i=1}^k c_i > 0, \quad k = 1, \dots, N-1, \\ c_i &= 2h_i \sqrt{1 + \frac{i\omega\mu\sigma_i}{\lambda^2}}, \quad i = 1, \dots, N-1. \end{aligned} \quad (13)$$

Proof. In order to demonstrate (12), starting from $j = 1$, by induction we show that

$$R_{N-j} = \sum_{k=1}^j \delta_k^{(N-j)} \exp(-(\gamma_{N+k-(j+1)} - \gamma_{N-(j+1)})\lambda), \quad \text{for } j = 1, \dots, N-1, \quad (14)$$

in which $\gamma_0 = 0$. We first observe that

$$2u_i h_i = 2h_i \sqrt{\lambda^2 + i\omega\mu\sigma_i} = 2h_i \sqrt{1 + \frac{i\omega\mu\sigma_i}{\lambda^2}} \cdot \lambda = c_i \lambda.$$

Let $j = 1$. By (6) and defining

$$\delta_1^{(N-1)} = \Psi_N = \frac{\sqrt{\lambda^2 - k_{N-1}^2} - \sqrt{\lambda^2 - k_N^2}}{\sqrt{\lambda^2 - k_{N-1}^2} + \sqrt{\lambda^2 - k_N^2}}, \quad (15)$$

we have that (14) is correct for $j = 1$ because $R_N = 0$. Assuming that (14) is also correct for a given $j < N - 1$, by (6)

$$\begin{aligned} R_{N-(j+1)} &= \frac{R_{N-j} + \Psi_{N-j}}{R_{N-j}\Psi_{N-j} + 1} e^{-c_{N-(j+1)}\lambda} \\ &= \sum_{k=1}^{j+1} \delta_k^{(N-(j+1))} \exp(-(\gamma_{N+k-(j+2)} - \gamma_{N-(j+2)})\lambda), \end{aligned} \quad (16)$$

in which we have defined

$$\begin{aligned} \delta_1^{(N-(j+1))} &= \frac{\Psi_{N-j}}{R_{N-j}\Psi_{N-j} + 1}, \\ \delta_k^{(N-(j+1))} &= \frac{\delta_{k-1}^{(N-j)}}{R_{N-j}\Psi_{N-j} + 1}, \quad k = 2, \dots, j+1. \end{aligned} \quad (17)$$

Finally, setting $\delta_j = \delta_j^{(1)}$, $j = 1, \dots, N - 1$, we obtain the result. ■

Lemma 3 For $\lambda \rightarrow +\infty$,

$$R_1 = \sum_{k=1}^{N-1} \frac{k_{k+1}^2 - k_k^2}{4\lambda^2} \left(1 + \mathcal{O}\left(\frac{1}{\lambda^2}\right) \right) \exp(-\gamma_k \lambda). \quad (18)$$

Proof. Starting from $j = 1$, by induction we show that

$$R_{N-j} = \sum_{k=1}^j \frac{k_{N+k-j}^2 - k_{N+k-(j+1)}^2}{4\lambda^2} \left(1 + \mathcal{O}\left(\frac{1}{\lambda^2}\right) \right) \exp(-(\gamma_{N+k-(j+1)} - \gamma_{N-(j+1)})\lambda), \quad (19)$$

for $j = 1, \dots, N - 1$. We observe that, for $i = 1, \dots, N$

$$\begin{aligned} \Psi_i &= \frac{\sqrt{\lambda^2 - k_{i-1}^2} - \sqrt{\lambda^2 - k_i^2}}{\sqrt{\lambda^2 - k_{i-1}^2} + \sqrt{\lambda^2 - k_i^2}} \\ &= \frac{k_i^2 - k_{i-1}^2}{\left[\lambda \left(1 + \frac{k_{i-1}^2}{2\lambda^2} + \mathcal{O}\left(\frac{1}{\lambda^4}\right) \right) + \lambda \left(1 + \frac{k_i^2}{2\lambda^2} + \mathcal{O}\left(\frac{1}{\lambda^4}\right) \right) \right]^2} \\ &= \frac{k_i^2 - k_{i-1}^2}{4\lambda^2 \left(1 + \mathcal{O}\left(\frac{1}{\lambda^2}\right) \right)} = \frac{k_i^2 - k_{i-1}^2}{4\lambda^2} \left(1 + \mathcal{O}\left(\frac{1}{\lambda^2}\right) \right). \end{aligned}$$

By (14) with $j = 1$ and (15), we have that

$$\begin{aligned} R_{N-1} &= \delta_1^{(N-1)} \exp(-(\gamma_{N-1} - \gamma_{N-2})\lambda) \\ &= \frac{k_N^2 - k_{N-1}^2}{4\lambda^2} \left(1 + \mathcal{O}\left(\frac{1}{\lambda^2}\right) \right) \exp(-(\gamma_{N-1} - \gamma_{N-2})\lambda). \end{aligned}$$

Therefore, (19) holds true for $j = 1$. Assuming that (19) is also correct for a given $j < N - 1$, by (16) we have

$$R_{N-(j+1)} = \sum_{k=1}^{j+1} \delta_k^{(N-(j+1))} \exp(-(\gamma_{N+k-(j+2)} - \gamma_{N-(j+2)})\lambda),$$

where by (17) and using the induction hypothesis on R_{N-j}

$$\begin{aligned} \delta_1^{(N-(j+1))} &= \frac{\Psi_{N-j}}{R_{N-j}\Psi_{N-j} + 1} \\ &= \frac{\frac{k_{N-j}^2 - k_{N-j-1}^2}{4\lambda^2} (1 + \mathcal{O}(\frac{1}{\lambda^2}))}{\mathcal{O}(\frac{1}{\lambda^2}) \frac{k_{N-j}^2 - k_{N-j-1}^2}{4\lambda^2} (1 + \mathcal{O}(\frac{1}{\lambda^2})) + 1} \\ &= \frac{k_{N-j}^2 - k_{N-j-1}^2}{4\lambda^2} \left(1 + \mathcal{O}\left(\frac{1}{\lambda^2}\right)\right), \\ \delta_k^{(N-(j+1))} &= \frac{\delta_{k-1}^{(N-j)}}{R_{N-j}\Psi_{N-j} + 1} \\ &= \frac{\frac{k_{N+k-(j+1)}^2 - k_{N+k-(j+2)}^2}{4\lambda^2} (1 + \mathcal{O}(\frac{1}{\lambda^2}))}{\mathcal{O}(\frac{1}{\lambda^2}) \frac{k_{N+k-(j+1)}^2 - k_{N+k-(j+2)}^2}{4\lambda^2} (1 + \mathcal{O}(\frac{1}{\lambda^2})) + 1} \\ &= \frac{k_{N+k-(j+1)}^2 - k_{N+k-(j+2)}^2}{4\lambda^2} \left(1 + \mathcal{O}\left(\frac{1}{\lambda^2}\right)\right), \quad k = 2, \dots, j+1. \end{aligned}$$

■

Using the above Lemmas we can prove the following result, which finally expresses the asymptotic behavior of R_1 , and hence of $R_0 - \Psi_1$ by Lemma 1.

Proposition 1 For $\lambda \rightarrow +\infty$,

$$R_1 = \sum_{k=1}^{N-1} \frac{k_{k+1}^2 - k_k^2}{4\lambda^2} \exp(-\tilde{\gamma}_k \lambda) \left(1 + \mathcal{O}\left(\frac{1}{\lambda}\right)\right), \quad (20)$$

where $\tilde{\gamma}_k = 2 \sum_{i=1}^k h_i$.

Proof. First of all, by (13) we have

$$\gamma_k = \sum_{i=1}^k c_i = 2 \sum_{i=1}^k h_i \left(1 + \mathcal{O}\left(\frac{1}{\lambda^2}\right)\right) = \tilde{\gamma}_k \left(1 + \mathcal{O}\left(\frac{1}{\lambda^2}\right)\right), \quad \text{for } k = 1, \dots, N-1. \quad (21)$$

Therefore

$$\begin{aligned} \exp(-\gamma_k \lambda) &= \exp\left(-\tilde{\gamma}_k \lambda \left(1 + \mathcal{O}\left(\frac{1}{\lambda^2}\right)\right)\right) \\ &= \exp(-\tilde{\gamma}_k \lambda) \left(1 + \mathcal{O}\left(\frac{1}{\lambda}\right)\right), \end{aligned}$$

where the last equality comes from

$$\exp\left(-\tilde{\gamma}_k \mathcal{O}\left(\frac{1}{\lambda}\right)\right) = 1 + \mathcal{O}\left(\frac{1}{\lambda}\right).$$

The result then follows straightfully from Lemma 3. ■

By Lemma 1 and Proposition 1, we have that the functions g_l , which are the integrand functions in (9) and (10), can be written as

$$\begin{aligned} g_l &= (R_0 - \Psi_1)\lambda^2 J_l(\lambda r) \\ &= \sum_{k=1}^{N-1} \frac{k_{k+1}^2 - k_k^2}{4} \exp(-\tilde{\gamma}_k \lambda) J_l(\lambda r) \left(1 + \mathcal{O}\left(\frac{1}{\lambda}\right)\right), \end{aligned} \quad (22)$$

so that the oscillations due to the Bessel functions are rapidly damped.

Just to provide an example, in Figure 2 we plot the imaginary part of $g_1(\lambda)$ and $q_1(\lambda)$ for a given model. It is clear that the oscillations are only retained by the term $q_1(\lambda)$.

This situation holds true in general and therefore, for suitable positive scalars s_l , $l = 0, 1$, we can consider the following approximations

$$H_z^{(N)} \approx \frac{m}{4\pi} \int_0^{s_0} g_0(\lambda) d\lambda + H_z^{(1)}, \quad (23)$$

$$H_\rho^{(N)} \approx -\frac{m}{4\pi} \int_0^{s_1} g_1(\lambda) d\lambda + H_\rho^{(1)}, \quad (24)$$

in which we neglect the tail of the integrals.

Theoretically, the truncation error can be bounded as follows.

Proposition 2 *For $l = 0, 1$ there exists a constant c such that, for s_l large enough,*

$$\left| \int_{s_l}^{\infty} g_l(\lambda) d\lambda \right| \leq c \sqrt{\frac{1}{8\pi r}} \sum_{k=1}^{N-1} |k_{k+1}^2 - k_k^2| \tilde{\gamma}_k^{-1} e^{-\tilde{\gamma}_k s_l} s_l^{-\frac{1}{2}}. \quad (25)$$

In order to prove Proposition 2 we need the following lemma.

Lemma 4 *For $u \rightarrow +\infty$,*

$$\int_u^{\infty} e^{-x} x^{-\nu} dx = u^{-\nu} e^{-u} \left(1 + \mathcal{O}\left(\frac{1}{u}\right)\right).$$

Proof. By using [13, pag.318] and [1, pag.505-504] respectively, we have that

$$\begin{aligned} \int_u^{\infty} \frac{e^{-x}}{x^\nu} dx &= u^{-\frac{\nu}{2}} e^{-\frac{u}{2}} \mathcal{W}_{-\frac{\nu}{2}, \frac{1-\nu}{2}}(u) \\ &= u^{1-\nu} e^{-u} \mathcal{U}(1, 2-\nu, u) \\ &= u^{-\nu} e^{-u} \left(1 + \mathcal{O}\left(\frac{1}{u}\right)\right), \end{aligned}$$

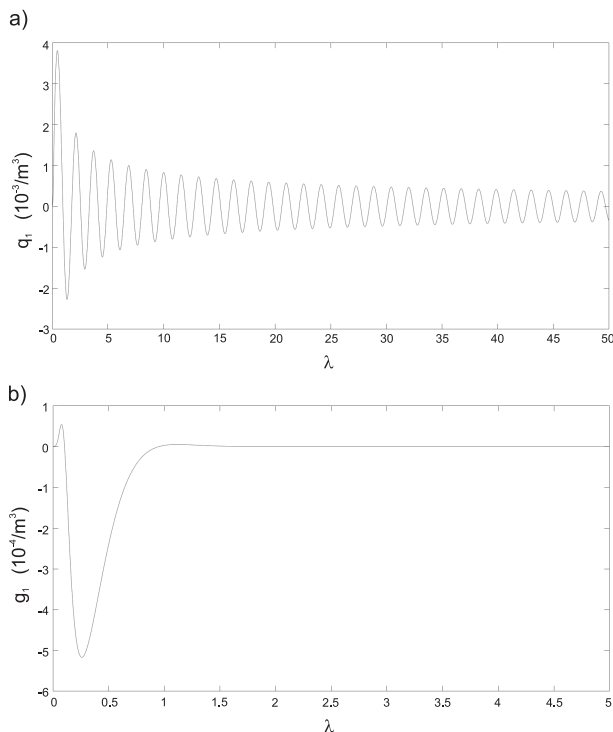


Figure 2: (a) The imaginary part of the function $q_1(\lambda)$ and (b) the imaginary part of the function $g_1(\lambda)$, in the case of a 3-layered underground model with $r = 2$ m, $f = 10$ kHz, $m = 1$ A/m², $\sigma_1 = 33$ mS/m, $\sigma_2 = 20$ mS/m, $\sigma_3 = 100$ mS/m, $h_1 = 2.5$ m, $h_2 = 0.5$ m.

where \mathcal{W} is the Whittaker function and \mathcal{U} is the Kummer's confluent hypergeometric function. ■

Now we can prove Proposition 2.

Proof. By (22) for $l = 0, 1$, we have

$$\left| \int_{s_l}^{\infty} g_l(\lambda) d\lambda \right| \lesssim \sum_{k=1}^{N-1} \frac{|k_{k+1}^2 - k_k^2|}{4} \int_{s_l}^{\infty} e^{-\tilde{\gamma}_k \lambda} |J_l(\lambda r)| d\lambda$$

Using the relation (see [1, pag.364])

$$J_l(t) = \sqrt{\frac{2}{\pi t}} \left[\cos \left(t - \frac{1}{2} l \pi - \frac{1}{4} \pi \right) + \mathcal{O} \left(\frac{1}{t} \right) \right], \quad \text{for } t \rightarrow +\infty,$$

s_l (m^{-1})	$\int_0^{s_0} g_0(\lambda) d\lambda$ (A/m)	$\int_0^{s_1} g_1(\lambda) d\lambda$ (A/m)
0.5	$-0.0871 \cdot 10^{-3}$	$0.2797 \cdot 10^{-3}$
1.0	$-0.1279 \cdot 10^{-3}$	$0.3279 \cdot 10^{-3}$
1.5	$-0.1316 \cdot 10^{-3}$	$0.3283 \cdot 10^{-3}$
2.0	$-0.1317 \cdot 10^{-3}$	$0.3281 \cdot 10^{-3}$
2.5	$-0.1317 \cdot 10^{-3}$	$0.3280 \cdot 10^{-3}$
3.0	$-0.1317 \cdot 10^{-3}$	$0.3280 \cdot 10^{-3}$
3.5	$-0.1317 \cdot 10^{-3}$	$0.3280 \cdot 10^{-3}$
4.0	$-0.1317 \cdot 10^{-3}$	$0.3280 \cdot 10^{-3}$

Table 1: Results of the Gauss-Kronrod quadrature for different values of s_l , with $r = 2 m$ and $f = 10 kHz$, in the case of a subsurface model composed by 3 layers: $\sigma_1 = 333 mS/m$, $\sigma_2 = 20 mS/m$, $\sigma_3 = 100 mS/m$, $h_1 = 2.5 m$, $h_2 = 0.5 m$.

and Lemma 4, we obtain

$$\begin{aligned}
\int_{s_l}^{\infty} e^{-\tilde{\gamma}_k \lambda} |J_l(\lambda r)| d\lambda &\lesssim \sqrt{\frac{2}{\pi r}} \int_{s_l}^{\infty} e^{-\tilde{\gamma}_k \lambda} \lambda^{-\frac{1}{2}} d\lambda \\
&= \sqrt{\frac{2}{\pi r}} \int_{\tilde{\gamma}_k s_l}^{\infty} e^{-t} t^{-\frac{1}{2}} dt \\
&\approx \sqrt{\frac{2}{\pi r}} \tilde{\gamma}_k^{-1} e^{-\tilde{\gamma}_k s_l} s_l^{-\frac{1}{2}},
\end{aligned}$$

where we have used the symbols \approx and \lesssim to neglect the factor $1 + \mathcal{O}(\frac{1}{\lambda})$. ■

In practice, s_l can be taken relatively small to obtain reliable results by a traditional quadrature formula on finite intervals, e.g., $s_l = 2 \div 3$, for $l = 0, 1$. Table 1 shows, for example, the results obtained with $r = 2 m$ and $f = 10 kHz$, in the case of a subsurface model composed by 3 layers: $\sigma_1 = 333 mS/m$, $\sigma_2 = 20 mS/m$, $\sigma_3 = 100 mS/m$, $h_1 = 2.5 m$, $h_2 = 0.5 m$. In Table 1, as well as in the sequel of this work, for the integral evaluation we have used the Gauss-Kronrod quadrature technique [25], with relative error tolerance equal to 10^{-8} . By adopting the above model, we also compared the fields $H_z^{(3)}$ and $H_\rho^{(3)}$, computed from the integral formulations (23) and (24), with the results of the digital filtering algorithm provided by Singh and Mogi [27]. Using 300 points, $s_0 = s_1 = 3$, and a tolerance equal to 10^{-9} for the integral evaluations, the two curves differ by less than 10^{-8} . Using more points the error further decreases, but with higher computational costs.

4 Approximation of the fields

In this section, working with $N = 2$ and $N = 3$, we derive useful analytical approximations for $H_z^{(N)}$ and $H_\rho^{(N)}$, expressed by equations (9) and (10). While these approximations can be used in general to have an idea of the main features of the fields, our basic aim is to use them for the inversion problem. First, from (11) we have that

$$g_l(\lambda) = \frac{4R_1 u_1}{R_1 k_1^2 + (\lambda + u_1)^2} \lambda^3 J_l(\lambda r), \quad l = 0, 1.$$

Before going on, we observe that for $0 \leq i, j, \ell \leq N$

$$\begin{aligned} (u_i - u_j) e^{-2u_\ell h_\ell} &= \frac{k_j^2 - k_i^2}{\sqrt{\lambda^2 - k_i^2} + \sqrt{\lambda^2 - k_j^2}} e^{-2\sqrt{\lambda^2 - k_i^2} h_\ell} \\ &= \mathcal{O}\left(\frac{e^{-2\lambda h_\ell}}{\lambda}\right) \quad \text{for } \lambda \rightarrow \infty \end{aligned} \quad (26)$$

and the same holds for $(\lambda - u_j) e^{-2u_\ell h_\ell}$. Actually, this asymptotic behavior is observed already for λ relatively small, because also the quantities k_i are very small. In order to derive approximations of $H_z^{(N)}$ and $H_\rho^{(N)}$, in what follows, whenever possible we neglect the terms involving these factors.

4.1 The case $N = 2$

For $N = 2$ we have

$$R_2 = 0, \quad R_1 = \Psi_2 e^{-2u_1 h_1} = \frac{u_1 - u_2}{u_1 + u_2} e^{-2u_1 h_1},$$

and therefore

$$\frac{4R_1 u_1}{R_1 k_1^2 + (\lambda + u_1)^2} = \frac{4u_1(u_1 - u_2)}{(\lambda^2 - u_1^2)(u_1 - u_2) e^{-2u_1 h_1} + (\lambda + u_1)^2 (u_1 + u_2)} e^{-2u_1 h_1}.$$

By (26) we can consider the approximation

$$(\lambda^2 - u_1^2)(u_1 - u_2) e^{-2u_1 h_1} \approx 0.$$

Moreover, using the first order approximation

$$u_1 = \sqrt{\lambda^2 + i\omega\mu\sigma_1} = \lambda \sqrt{1 + \frac{i\omega\mu\sigma_1}{\lambda^2}} \approx \lambda \left(1 + \frac{i\omega\mu\sigma_1}{2\lambda^2}\right), \quad (27)$$

we obtain

$$\frac{4R_1 u_1}{R_1 k_1^2 + (\lambda + u_1)^2} \approx \frac{4u_1(u_1 - u_2)}{(\lambda + u_1)^2 (u_1 + u_2)} e^{-2u_1 h_1} \quad (28)$$

$$= \frac{4u_1(u_1 - u_2)^2 (\lambda - u_1)^2}{(\lambda^2 - u_1^2)^2 (u_1^2 - u_2^2)} e^{-2u_1 h_1} \quad (29)$$

$$\approx \frac{i\omega\mu(\sigma_1 - \sigma_2)}{4\lambda^3} \left(1 + \frac{i\omega\mu\sigma_1}{2\lambda^2}\right) e^{-2u_1 h_1}. \quad (30)$$

At this point, we use the non standard approximation

$$u_1 = \sqrt{\lambda^2 + i\omega\mu\sigma_1} \approx \lambda + \sqrt{i\omega\mu\sigma_1}. \quad (31)$$

The main reason for this choice is that the standard (27) leads to final approximation that does not allow to simplify the integrals with the existing formulas. Anyway the approximation (31) is partially justified by observing that

$$\frac{u_1}{\lambda + \sqrt{i\omega\mu\sigma_1}} \rightarrow 1, \quad \text{for } \lambda \rightarrow 0 \text{ and } \lambda \rightarrow +\infty.$$

Now, since

$$\lambda + \sqrt{i\omega\mu\sigma_1} = \lambda + \frac{\sqrt{2}}{2}\sqrt{\omega\mu\sigma_1} + i\frac{\sqrt{2}}{2}\sqrt{\omega\mu\sigma_1},$$

we obtain

$$\begin{aligned} e^{-2u_1 h_1} &\approx e^{-2\lambda h_1 - h_1 \sqrt{2\omega\mu\sigma_1}} [\cos(h_1 \sqrt{2\omega\mu\sigma_1}) - i \sin(h_1 \sqrt{2\omega\mu\sigma_1})] \\ &\approx e^{-2\lambda h_1 - h_1 \sqrt{2\omega\mu\sigma_1}}. \end{aligned}$$

Using the above approximation in (30) we have

$$\Im \left(\frac{4R_1 u_1}{R_1 k_1^2 + (\lambda + u_1)^2} \right) \approx \frac{\omega\mu(\sigma_1 - \sigma_2) e^{-2\lambda h_1 - h_1 \sqrt{2\omega\mu\sigma_1}}}{4\lambda^3}.$$

where the symbol \Im indicates the imaginary part. Moreover, by the general formula (see [13], p. 707)

$$\int_0^\infty e^{-\alpha x} J_\nu(\beta x) dx = \frac{\beta^{-\nu} [\sqrt{\alpha^2 + \beta^2} - \alpha]^\nu}{\sqrt{\alpha^2 + \beta^2}}, \quad \Re(\nu) > -1, \Re(\alpha \pm i\beta) > 0,$$

where the symbol \Re indicates the real part. We finally obtain, for the integral in equation (9), the following approximation:

$$\begin{aligned} \Im \left(\int_0^\infty \frac{4R_1 u_1}{R_1 k_1^2 + (\lambda + u_1)^2} \lambda^3 J_0(\lambda r) d\lambda \right) &\approx \frac{\omega\mu(\sigma_1 - \sigma_2) e^{-h_1 \sqrt{2\omega\mu\sigma_1}}}{4} \int_0^\infty e^{-2\lambda h_1} J_0(\lambda r) d\lambda \\ &= \frac{\omega\mu(\sigma_1 - \sigma_2) e^{-h_1 \sqrt{2\omega\mu\sigma_1}}}{4\sqrt{4h_1^2 + r^2}}. \end{aligned}$$

Using the same arguments for $H_\rho^{(2)}$, the integral in equation (10) can be approximated as

$$\begin{aligned} &\Im \left(\int_0^\infty \frac{-4R_1 u_1}{R_1 k_1^2 + (\lambda + u_1)^2} \lambda^3 J_1(\lambda r) d\lambda \right) \approx \\ &\approx -\frac{\omega\mu(\sigma_1 - \sigma_2) e^{-h_1 \sqrt{2\omega\mu\sigma_1}}}{4} \int_0^\infty e^{-2\lambda h_1} J_1(\lambda r) d\lambda \\ &= -\frac{\omega\mu(\sigma_1 - \sigma_2) e^{-h_1 \sqrt{2\omega\mu\sigma_1}} (\sqrt{4h_1^2 + r^2} - 2h_1)}{4r\sqrt{4h_1^2 + r^2}}. \end{aligned}$$

Finally,

$$\mathfrak{S}(H_z^{(2)}) \approx \frac{m}{4\pi} \left(\frac{\omega\mu(\sigma_1 - \sigma_2)e^{-h_1\sqrt{2\omega\mu\sigma_1}}}{4\sqrt{4h_1^2 + r^2}} \right) + \mathfrak{S}(H_z^{(1)})$$

and

$$\mathfrak{S}(H_\rho^{(2)}) \approx -\frac{m}{4\pi} \left(\frac{\omega\mu(\sigma_1 - \sigma_2)e^{-h_1\sqrt{2\omega\mu\sigma_1}}(\sqrt{4h_1^2 + r^2} - 2h_1)}{4r\sqrt{4h_1^2 + r^2}} \right) + \mathfrak{S}(H_\rho^{(1)}).$$

4.2 The case $N = 3$

For $N = 3$ we have

$$\begin{aligned} R_3 &= 0, \\ R_2 &= \Psi_3 e^{-2u_2 h_2} = \frac{u_2 - u_3}{u_2 + u_3} e^{-2u_2 h_2}, \\ R_1 &= \frac{\frac{u_2 - u_3}{u_2 + u_3} e^{-2u_2 h_2} + \frac{u_1 - u_2}{u_1 + u_2} e^{-2u_1 h_1}}{\frac{u_2 - u_3}{u_2 + u_3} \frac{u_1 - u_2}{u_1 + u_2} e^{-2u_2 h_2} + 1} e^{-2u_1 h_1} \\ &= \frac{(u_1 + u_2)(u_2 - u_3)e^{-2u_2 h_2} + (u_1 - u_2)(u_2 + u_3)e^{-2u_1 h_1}}{(u_2 - u_3)(u_1 - u_2)e^{-2u_2 h_2} + (u_1 + u_2)(u_2 + u_3)} \\ &\approx \frac{(u_1 + u_2)(u_2 - u_3)e^{-2u_2 h_2} + (u_1 - u_2)(u_2 + u_3)e^{-2u_1 h_1}}{(u_1 + u_2)(u_2 + u_3)}, \end{aligned}$$

where, as before, we have used (26). We obtain

$$\begin{aligned} \frac{4R_1 u_1}{R_1 k_1^2 + (\lambda + u_1)^2} &= 4u_1 [(u_1 + u_2)(u_2 - u_3)e^{-2(u_1 h_1 + u_2 h_2)} + (u_1 - u_2)(u_2 + u_3)e^{-2u_1 h_1}] \times \\ &\quad [(u_1 + u_2)(u_2 - u_3)(\lambda^2 - u_1^2)e^{-2(u_1 h_1 + u_2 h_2)} + (u_1 - u_2)(u_2 + u_3)(\lambda^2 - u_1^2)e^{-2u_1 h_1} \\ &\quad + (\lambda + u_1)^2 (u_1 - u_2)(u_2 - u_3)e^{-2u_2 h_2} + (\lambda + u_1)^2 (u_1 + u_2)(u_2 + u_3)]^{-1} \\ &\approx 4u_1 \frac{(u_1 + u_2)(u_2 - u_3)e^{-2(u_1 h_1 + u_2 h_2)} + (u_1 - u_2)(u_2 + u_3)e^{-2u_1 h_1}}{(\lambda + u_1)^2 (u_1 + u_2)(u_2 + u_3)} \end{aligned} \quad (32)$$

$$= \frac{4u_1(u_2 - u_3)e^{-2(u_1 h_1 + u_2 h_2)}}{(\lambda + u_1)^2 (u_2 + u_3)} + \frac{4u_1(u_1 - u_2)e^{-2u_1 h_1}}{(\lambda + u_1)^2 (u_1 + u_2)}, \quad (33)$$

where the approximation (32) arises again from (26). We observe that the two terms of (33) are very similar and, in particular, the second one corresponds to (28) for $N = 2$. Therefore, using the approximations (27) and (31) for u_1 , u_2 and u_3 , we obtain

$$\begin{aligned} &\mathfrak{S} \left(\int_0^\infty \frac{4R_1 u_1}{R_1 k_1^2 + (\lambda + u_1)^2} \lambda^3 J_0(\lambda r) d\lambda \right) \approx \\ &\approx \frac{\omega\mu e^{-h_1\sqrt{2\omega\mu\sigma_1}}}{4} \left(\frac{(\sigma_2 - \sigma_3)e^{-h_2\sqrt{2\omega\mu\sigma_2}}}{\sqrt{4(h_1 + h_2)^2 + r^2}} + \frac{\sigma_1 - \sigma_2}{\sqrt{4h_1^2 + r^2}} \right). \end{aligned}$$

Analogously,

$$\begin{aligned} & \Im \left(\int_0^\infty \frac{-4R_1 u_1}{R_1 k_1^2 + (\lambda + u_1)^2} \lambda^3 J_1(\lambda r) d\lambda \right) \approx \\ & \approx \frac{\omega \mu e^{-h_1 \sqrt{2\omega \mu \sigma_1}}}{-4r} \left(\frac{(\sigma_2 - \sigma_3) e^{-h_2 \sqrt{2\omega \mu \sigma_2}} [\sqrt{4(h_1 + h_2)^2 + r^2} - 2(h_1 + h_2)]}{\sqrt{4(h_1 + h_2)^2 + r^2}} \right. \\ & \left. + \frac{(\sqrt{4h_1^2 + r^2} - 2h_1)(\sigma_1 - \sigma_2)}{\sqrt{4h_1^2 + r^2}} \right). \end{aligned}$$

Finally,

$$\Im(H_z^{(3)}) \approx \frac{m}{4\pi} \frac{\omega \mu e^{-h_1 \sqrt{2\omega \mu \sigma_1}}}{4} \left(\frac{(\sigma_2 - \sigma_3) e^{-h_2 \sqrt{2\omega \mu \sigma_2}}}{\sqrt{4(h_1 + h_2)^2 + r^2}} + \frac{\sigma_1 - \sigma_2}{\sqrt{4h_1^2 + r^2}} \right) + \Im(H_z^{(1)}) \quad (34)$$

and

$$\begin{aligned} \Im(H_\rho^{(3)}) \approx & -\frac{m}{4\pi} \frac{\omega \mu e^{-h_1 \sqrt{2\omega \mu \sigma_1}}}{4r} \left(\frac{(\sigma_2 - \sigma_3) e^{-h_2 \sqrt{2\omega \mu \sigma_2}} [\sqrt{4(h_1 + h_2)^2 + r^2} - 2(h_1 + h_2)]}{\sqrt{4(h_1 + h_2)^2 + r^2}} \right. \\ & \left. + \frac{(\sqrt{4h_1^2 + r^2} - 2h_1)(\sigma_1 - \sigma_2)}{\sqrt{4h_1^2 + r^2}} \right) + \Im(H_\rho^{(1)}). \end{aligned} \quad (35)$$

5 The inverse problem

Let $p = (\sigma_1, \dots, \sigma_N, h_1, \dots, h_{N-1}) \in \mathbb{R}^{2N-1}$ be the vector of underground parameters. The components of the magnetic field at the surface are functions of these parameters and the offset r , thus $H_z^{(N)} = H_z^{(N)}(p, r)$ and $H_\rho^{(N)} = H_\rho^{(N)}(p, r)$. Given a vector of observations $d = (d_{z,1}, \dots, d_{z,k}, d_{\rho,1}, \dots, d_{\rho,k})^T$, corresponding to distances r_1, \dots, r_k ($2k > 2N - 1$), the inverse problem can be formulated as

$$\min_p \sum_{i=1}^k \left\{ \left[\Im(H_z^{(N)}(p, r_i)) - d_{z,i} \right]^2 + \left[\Im(H_\rho^{(N)}(p, r_i)) - d_{\rho,i} \right]^2 \right\}. \quad (36)$$

It is known that other kind of minimizations are possible, that is, by using a different norm, and eventually a regularization term can be included to reduce the effect of noise on the measurements. By defining $\mathcal{H} : \mathbb{R}^{2N-1} \rightarrow \mathbb{R}^{2k}$ as

$$\mathcal{H}(p) = \left(\Im(H_z^{(N)}(p, r_1)), \dots, \Im(H_z^{(N)}(p, r_k)), \Im(H_\rho^{(N)}(p, r_1)), \dots, \Im(H_\rho^{(N)}(p, r_k)) \right)^T, \quad (37)$$

the problem (36) can be rewritten in the compact form

$$\min_p \|\mathcal{H}(p) - d\|^2. \quad (38)$$

Due to the complexity of the function $\mathcal{H}(p)$, whose computation requires the evaluation of integrals, it is necessary to employ a derivative free minimization algorithms based, for example, on a BFGS line-search method ([4, 8, 12, 26]) and on the SA global-search technique ([19, 11]). However, these methods are very demanding in terms of computational resources and elaboration time. By using the approximations given in the previous section, below we present a more efficient algorithm to solve (38) in the nontrivial case of $N = 3$.

Let $p = (\sigma_1, \sigma_2, \sigma_3, h_1, h_2) \in \mathbb{R}^5$ be the vector of the underground parameters and consider the fields $H_z^{(3)} = H_z$ and $H_\rho^{(3)} = H_\rho$, defined by equations (9) and (10). From the previous section, $\Im(H_z)$ and $\Im(H_\rho)$ can be approximated using equations (34) and (35) at different offsets r_1, \dots, r_k . We indicate these approximations as L_z and L_ρ .

Suppose a real underground model be characterized by the parameters vector $p^* = (\sigma_1^*, \sigma_2^*, \sigma_3^*, h_1^*, h_2^*) \in \mathbb{R}^5$. The observations vector d is computed using the integral formulations (23) and (24), being numerical simulations the best representation of realistic EM surveys. Given an initial guess p_0 of p^* , we search for a certain $\bar{p} \in \mathbb{R}^5$ such that

$$\bar{p} = (\bar{\sigma}_1, \bar{\sigma}_2, \bar{\sigma}_3, \bar{h}_1, \bar{h}_2) = \arg \min_p \|\bar{\mathcal{H}}(p) - d\|^2, \quad (39)$$

where $\bar{\mathcal{H}} : \mathbb{R}^5 \rightarrow \mathbb{R}^{2k}$ is defined as

$$\bar{\mathcal{H}}(p) = (L_z(p, r_1), \dots, L_z(p, r_k), L_\rho(p, r_1), \dots, L_\rho(p, r_k))^T.$$

At this point we use \bar{p} as initial guess for a second minimization procedure with the integral formulations (23) and (24) instead of the analytical approximations (34) and (35). Therefore, we look for $\hat{p} \in \mathbb{R}^5$ such that

$$\hat{p} = (\hat{\sigma}_1, \hat{\sigma}_2, \hat{\sigma}_3, \hat{h}_1, \hat{h}_2) = \arg \min_p \|\mathcal{H}(p) - d\|^2, \quad (40)$$

where $\mathcal{H} : \mathbb{R}^5 \rightarrow \mathbb{R}^{2k}$ is defined by (37). Finally, the approximate solution of the inverse problem is given by the vector $\hat{p} \in \mathbb{R}^5$.

The above procedure can be summarized by the following algorithm.

Algorithm 1 Given $p_0 \in \mathbb{R}^5$ and $d \in \mathbb{R}^{2k}$,

1. solve the problem (39) to find \bar{p} ,
2. solve the problem (40), with \bar{p} as initial guess, to find \hat{p} .

Since $\bar{\mathcal{H}}(p) \approx \mathcal{H}(p)$ is a good approximation (see the examples in the following section), the double step minimization allows to considerably reduce the computational cost because $\bar{\mathcal{H}}$ does not require the evaluation of integrals.

	$\sigma(S/m)$
Clay	0.2 [6]
Sand/Silt grains	0.01 [6]
Tap water	0.1 [28]
Air	0.0001 [23]

Table 2: Material electrical conductivity

6 Examples

In this section we present the results obtained by implementing the Algorithm 1, using the BFGS optimization solver. We compare these results with the solutions provided by the SA optimization solver. The examples aim to simulate an EM acquisition on river levees using the DUALEM system (<https://dualem.com>), for which the offsets are $r_1 = 2 m$, $r_2 = 4 m$, $r_3 = 6 m$ and $r_4 = 8 m$, and the frequency is about $f = 10 kHz$.

6.1 Conductivity models of river levees

Regarding the choice of the underground models, we considered a specific application related to the internal composition of river levees, which may collapse due to the condition of the soils that form the embankments. Particularly, the presence of gravel lenses inside the embankment body constitutes a critical factor for the structural levee stability. Therefore, the subsoil models are composed by three layers, representing a highly porous gravel level embedded in sediments composed by clay and silty sands. Two (extreme) cases are considered: the first case (Models 1 and 3) represents a dry levee (summer conditions) and the second case (Models 2 and 4) represents a wet levee (winter conditions). Moreover, different layer thicknesses are taken into account. The layer conductivities are computed with the complex refractive index model (CRIM), described in A, and the material properties shown in Table 2 and Table 3. The computed values in Table 3 represent typical conductivities of shallow sediments, frequently measured on river embankments (e.g., [32, 9]).

6.2 Results of the EM modelling and inversion

First of all, we compared the fields $H_z^{(N)}$ and $H_\rho^{(N)}$ computed adopting the numerical Gauss-Kronrod quadrature technique, the analytical approximation and the numerical digital filtering algorithm provided by Singh and Mogi [27]. Figure 3 shows the imaginary part of (23) and (24), with $N = 3$, and their analytical approximations (34) and (35), for both Model 1 and Model 2.

The two components of the the magnetic field correspond to the HCP and PRP coil configurations, respectively. The values computed using the numerical

Medium	Layer	C (%)	ϕ (%)	S_w (%)	σ (mS/m)	h (m)	Lithology
Model 1	1	50	20	3	50.0	2.5	Dry silt and clay
	2	1	37	1	4.9	0.5	Dry gravel lens
	3	25	30	2	18.2		Dry sand/silt and clay
Model 2	1	50	20	92	76.9	2.5	Wet silt and clay
	2	1	37	98	32.3	0.5	Wet gravel lens
	3	25	30	98	50.0		Wet sand/silt and clay
Model 3	1	50	20	3	50.0	3.0	Dry silt and clay
	2	1	37	1	4.9	2.0	Dry gravel lens
	3	25	30	2	18.2		Dry sand/silt and clay
Model 4	1	50	20	92	76.9	3.0	Wet silt and clay
	2	1	37	98	32.3	2.0	Wet gravel lens
	3	25	30	98	50.0		Wet sand/silt and clay

Table 3: Petrophysical properties of the river levees models used in the numerical forward simulations.

digital filter approach are shown as well. This plot confirms the very good concordance of the two numerical representations, whose difference was previously estimated by less than 10^{-8} . Moreover, the curves show that the analytical approximation is better for the PRP configuration.

To solve the minimization problems (39) and (40), we used the quasi-Newton method BFGS, with step tolerance and termination tolerance in the order of the machine precision. We applied the Algorithm 1 to the observations vector d obtained from the models defined in Table 3 and calculated the relative percentage error between the solution \hat{p} and the real underground model parameters p^* . We also applied the SA global-search technique to directly solve the minimization problem (40), i.e., without using the analytical approximations (34) and (35). In fact, this kind of technique do not benefit from the two-step procedure described in the previous section and schematized in Algorithm 1, because the final result does not depend on the initial model.

The observation data vector d is generated by

$$d = \mathcal{H}(p^*) + \eta,$$

where η is a random white noise vector such that the Noise-to-Signal Ratio (NSR) is $\epsilon = \frac{\|\eta\|}{\|d\|}$. We consider two values of percentage NSR , $\epsilon = 0.1\%$, 0.5% . These values are compatible with the results of laboratory test, showing that environmental RMS noise levels, in terms of apparent conductivity measurements at 8 m offset, are typically less than 1 mS/m (see <https://dualem.com>). The solution errors were averaged over 20 simulations for each model, in order

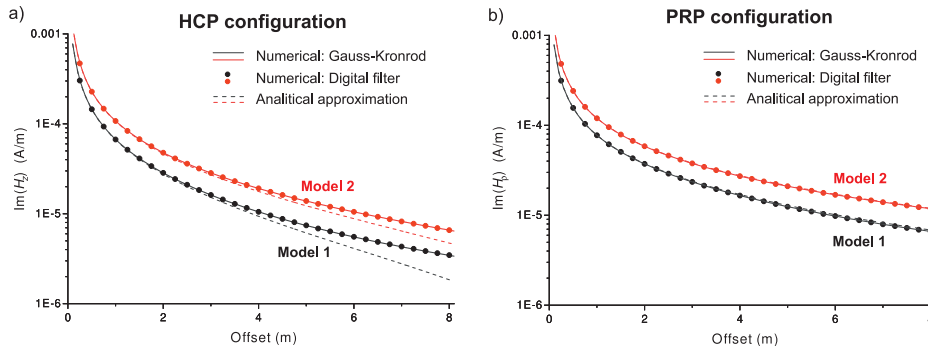


Figure 3: Comparison between the fields $H_z^{(3)}$ (a) and $H_\rho^{(3)}$ (b) computed adopting the numerical Gauss-Kronrod quadrature technique (solid lines), the analytical approximation (dashed lines) and the numerical digital filtering algorithm provided by Singh and Mogi [27] (symbols). The two components of the the magnetic field correspond to the HCP and PRP coil configurations, respectively. Both Model 1 and Model 2 are considered.

to have an estimate of the parameters expectation values.

For the SA optimization method, the initial temperature is 10^6 , the temperature reduction factor is 0.1 and the error tolerance for termination is 10^{-9} , without noise. By adding the random noise to the data, the error tolerance was increased to 10^{-6} . The lower and upper bounds are fixed, on the basis of observations of river levees carried out with other direct and indirect methods, to the following values: 3 mS/m and 1 S/m for the conductivity, and to 0.1 m and 4 m for the thickness.

The results of the simulations are shown in Tables 4-5-6, where we report the mean relative error over 20 experiments for each model in order to reduce the random dependence on the data. The optimization solvers always converge for all the simulations. The errors are mainly due to the presence of a large number of local minima in the objective function. The simulations without random noise (Table 4) show the best results, with the maximum average error around 5%. Then, as expected, the errors increase with increasing NSR , reaching an average maximum error of $\approx 35\%$ for $NSR = 0.5$ (Table 6). The conductivity and thickness of the intermediate layer are affected by the larger errors. The results of SA show very low errors on the top and bottom layers, while the errors related to the BFGS method are more homogeneously distributed on the three layers. Moreover, thinner layers show larger errors.

Overall, the performance of the two methods are very similar in terms of accuracy (see average errors at the bottom of Tables 4-5-6). In the absence of noise, the SA technique provides slightly lower errors than BFGS, while in pres-

	Mean relative error(<i>SA</i>)		Mean relative error(<i>BFGS</i>)	
	Conductivity (%)	Thickness (%)	Conductivity (%)	Thickness (%)
Model 1	0.0	0.13	0.1	0.0
	11.5	1.86	5.4	5.4
	0.02		0.1	
Model 2	0.0	0.26	0.1	0.2
	3.38	4.51	2.0	1.1
	0.01		0.1	
Model 3	0.0	0.0	0.7	1.0
	8.71	7.1	53.0	23.8
	1.26		1.8	
Model 4	0.0	1.21	0.0	0.3
	6.66	15.9	1.7	6.2
	0.45		0.5	
Average error	2.66	3.87	5.4	4.75

Table 4: Results of the EM inversions using the SA and BFGS methods. The NSR is $\epsilon = 0$.

ence of noise we observe the opposite behavior. However, it is very important to note that the Algorithm 1 with the BFGS optimization solver is more than 10 times faster than SA, requiring less than 1 s for a single inversion on a common laptop.

7 Conclusions

The numerical and analytical estimation of the electric and magnetic fields is at the basis of the modeling and inversion algorithms commonly used in induction EM methods. Here we present a novel methodology for the computation of the integrals involved in the solution of the Maxwell equations, based on the splitting of the reflection term. In this context, a classical quadrature rule on finite intervals can be applied. On the other hand, this approach also allows an analytical approximation of the integrals, that can be used to speed-up the solution of the inverse problems.

We have estimated the validity of our approach for the specific case of the DUALEM (DUAL-geometry Electro-Magnetic) system, but the physics is not restricted to these type of instruments. The specific examples consider the study of river-levees integrity, which is a very important environmental problem

	Mean relative error(SA)		Mean relative error(BFGS)	
	Conductivity (%)	Thickness (%)	Conductivity (%)	Thickness (%)
Model 1	0.34	2.0	16.3	11.2
	24.7	33.4	24.2	5.5
	1.90		9.2	
Model 2	0.53	5.95	8.3	9.5
	22.1	19.7	7.6	14.8
	4.16		2.6	
Model 3	0.09	0.87	9.4	7.5
	19.0	19.2	15.2	21.0
	5.38		3.4	
Model 4	0.09	4.81	5.2	4.0
	23.1	20.2	1.8	7.0
	8.9		6.2	
Average error	9.19	13.3	9.12	10.0

Table 5: Results of the EM inversions using the SA and BFGS methods. The NSR is $\epsilon = 0.1\%$.

	Mean relative error(SA)		Mean relative error(BFGS)	
	Conductivity (%)	Thickness (%)	Conductivity (%)	Thickness (%)
Model 1	1.0	9.56	21.0	16.2
	32.1	34.9	35.2	4.5
	8.66		12.6	
Model 2	0.43	8.23	11.0	13.2
	27.4	30.1	21.5	20.7
	5.19		4.5	
Model 3	0.37	5.01	16.7	12.3
	24.3	31.7	29.1	19.2
	13.7		4.8	
Model 4	0.37	12.4	15.7	11.6
	32.2	24.4	13.7	8.5
	12.6		18.4	
Average error	13.2	19.5	17.02	13.28

Table 6: Results of the EM inversions using the SA and BFGS methods. The NSR is $\epsilon = 0.5\%$

in Italy, due to the high hydrological risks.

A numerical algorithm based on the Gauss-Kronrod technique is used to compute the components of the EM field at low frequency in a stratified medium. The results are in good agreement with those of the commonly used digital filtering method. Moreover, the analytical approximation match well with the numerical solution both for resistive and conductive environments.

Two optimization algorithms are applied for the solution of the inverse problem, the line-search BFGS method, enhanced by the analytical approximation, and the global-search Simulated Annealing technique. The numerical experiments confirm the reliability of these techniques. Furthermore, while the two methods show similar performances in terms of solution accuracy, the former is more than 10 times faster than the latter. This asset of the enhanced BFGS method enables its application to the inversion of large datasets.

Although it is specific for the case of river levees, this analysis has a general validity, and allows to overcome the limits of common methods based on the modelling of apparent conductivity in the low induction number (LIN) approximation.

A Electrical conductivity

The subsoil conductivities are computed with the complex refractive index model (CRIM). The CRIM model for a shaly sandstone with negligible permittivity and partially saturated with gas, can be expressed as [24, 5]

$$\sigma = [(1-\phi)(1-C)\sigma_q^\gamma + (1-\phi)C\sigma_c^\gamma + \phi S_w\sigma_w^\gamma + \phi(1-S_w)\sigma_a^\gamma]^{1/\gamma}, \quad \gamma = 1/2 \quad (41)$$

where σ_q , σ_c , σ_w and σ_a are the sand-grain (quartz), clay, water and air conductivities, C is the clay content, ϕ is the porosity and S_w is the water saturation. If γ is a free parameter, the equation is termed Lichtnecker-Rother formula. It is based on the ray approximation. The travel time in each medium is inversely proportional to the electromagnetic velocity, which in turn is inversely proportional to the square root of the complex dielectric constant. At low frequencies, displacement currents can be neglected and equation (41) is obtained. For zero clay content, and neglecting σ_q and σ_c , equation (41) is exactly Archie's law [16].

Acknowledgements

This work was partially supported by GNCS-INdAM, FRA-University of Trieste and CINECA under HPC-TRES program award number 2019-04. This research was also supported by the DILEMMA project (Imaging, modelling, monitoring and design of earthen levees), funded by the "Ministero dell'Ambiente e della Tutela del Territorio e del Mare" (MATTM). Eleonora Denich and Paolo Novati are members of the INdAM research group GNCS.

References

- [1] M. Abramowitz and I. A. Stegun (1970), *Handbook of Mathematical Functions with Formulas, Graphs, and Mathematical Tables*, Dover Publications, Inc., New York.
- [2] Anderson, W.L. (1982), *Fast Hankel-transforms using related and lagged convolutions*, ACM Transactions on Mathematical Software, 8(4).
- [3] Anderson, W.L. (1979), *Computer Program: Numerical integration of related Hankel transforms of orders 0 and 1 by adaptive digital filtering*, Geophysics, 44(7).
- [4] Broyden, C. G. (1970), *The Convergence of a Class of Double-Rank Minimization Algorithms*, Journal Inst. Math. Applic.
- [5] Carcione J. M. (2014), *Wave fields in real media: Wave propagation in anisotropic, anelastic, porous and electromagnetic media*, Elsevier Science, Amsterdam, Handbook of Geophysical Exploration.
- [6] Carcione J. M., Gei D., Picotti S. and Michelini A. (2012), *Cross-hole electromagnetic and seismic modeling for CO₂ detection and monitoring in a saline aquifer*, Journal of Petroleum Science and Engineering.
- [7] Erdelyi, A., Ed. (1954), *Tables of Integral Transform*, McGraw-Hill Book Co.
- [8] Fletcher, R. (1970), *A New Approach to Variable Metric Algorithms*, Computer Journal.
- [9] Francese R., Morelli G., Santos F. M., Bondesan A., Giorgi M. and Tesarollo A. (2018), *An integrated geophysical approach to scan river embankments*, Fast Times, 23(3), 86-96.
- [10] Ghosh, D.P. (1971), *The application of linear filter theory to the direct interpretation of geoelectrical resistivity sounding measurements*, Geophysical Prospecting, 19(2), 192-217.
- [11] Goffe W. L., Ferrier G. D. and Rogers J. (1994), *Global optimization of statistical functions with Simulated Annealing*, Journal of Econometrics 60(1).
- [12] Goldfarb, D. (1970), *A Family of Variable Metric Updates Derived by Variational Means*, Mathematics of Computing, 24.
- [13] Gradshteyn, I. S. and Ryzhik, I. M. (1980), *Tables of Integrals, Series, and Products*, Academic Press, New York.
- [14] Guptasarma, D. (1982), *Optimization of short digital linear filters for increased accuracy*, Geophysical Prospecting 30, 501-514.

- [15] Guptasarma, D., Singh, B. (1997), *New digital linear filters for Hankel J_0 and J_1 transform*, Geophysical Prospecting 45.
- [16] Hoversten G. M., Cassassuce F., Gasperikova E., Newman G. A., Chen J., Rubin Y., Hou Z. and Vasco D. (2006), *Direct reservoir parameter estimation using joint inversion of marine seismic AVA and CSEM data.i*, Geophysics, 71(3), C1-C13.
- [17] Ingeman-Nielsen, T. and Baumgartner, F. (2006), *CR1Dmod: A Matlab program to model 1D complex resistivity effects in electrical and electromagnetic surveys*, Computer & Geosciences, 32, 1411-1419.
- [18] Johansen, H. K., and Sorensen, K. (1979), *Fast Hankel transforms*, Geophysical Prospecting, 27(4), 876-901.
- [19] Kirkpatrick S., Gelatt C. D. and Vecchi M. P. (1983), *Optimization by Simulated Annealing*, Science 4598(220).
- [20] Koefoed, O., and Dirks, F.J.H. (1979), *Determination of resistivity sounding filters by the Wiener-Hopf least-squares method*, Geophysical Prospecting, 27(1), 245-250.
- [21] Koefoed O., Ghosh, D. P., and Polman, G. J. (1972), *Computation of type curves for electromagnetic depth sounding with a horizontal transmitting coil by means of a digital linear filter*, Geophysical Prospecting, 20(2), 406-420.
- [22] Kong, F.N. (2007), *Hankel transform filters for dipole antenna radiation in a conductive medium*, Geophysical Prospecting.
- [23] Pawar S. D., Murugavel P. and Lal D. M. (2009), *Effect of relative humidity and sea level pressure on electrical conductivity of air over Indian Ocean*, Journal of Geophysical Research, 114(D2).
- [24] Schön J.H. (1996), *Physical properties of rocks*, Pergamon Press, Handbook of Geophysical Exploration.
- [25] Shampine, L.F. (2008), *Vectorized Adaptive Quadrature in MATLAB*, Journal of Computational and Applied Mathematics, 211, 131-140.
- [26] Shanno, D. F. (1970), *Conditioning of Quasi-Newton Methods for Function Minimization*, Mathematics of Computing.
- [27] Singh, N.P., Mogi, T. (2010), *EMDPLER: A F77 program for modelling the EM response of dipolar sources over the non-magnetic layer earth models*, Computer & Geosciences, 36, 430-440.
- [28] Ward S. H. and Hohmann G. W. (1987), *Resistivity characteristics of geologic targets*, In: Nabighian, M.N., (ed.), *Electromagnetic Methods in Applied Geophysics*, Tulsa, Oklahoma, 53-129.

- [29] Ward, S.H. and Hohmann, G.W. (1988), *Electromagnetic theory for geophysical applications*, In: Nabighian, M.N., (ed.), *Electromagnetic Methods in Applied Geophysics*, Tulsa, Oklahoma, pp 131-311.
- [30] Watson, G. N. (1966), *A treatise on the theory of Bessel functions*, Cambridge University press, 2nd. edition reprinted.
- [31] Werthmuller, D., Key, K., and Slob, E.C. (2018), *A tool for designing digital filters for the Hankel and Fourier transforms in potential, diffusive, and wavefield modeling*, *Geophysics*.
- [32] Zohdy A. A. R. and Jackson D. B. (1969), *Application of deep electrical soundings for groundwater exploration in Hawaii*, *Geophysics*, 34(4), 584-600.